Stability of Current-Sensorless Control of Permanent Magnet Synchronous Motors*

Jiunn-Jiang CHEN** and Kan-Ping CHIN**

This study applies Lyapunov's direct method to verify the stability of permanent magnet synchronous motors under singular perturbation control designs. The position and velocity controller designed herein does not require the current information of the motor for feedback purposes (current-sensorless), but the steady-state d-axis current can still be controlled to zero to minimize power dissipation. Combining Lyapunov's linearization stability analysis, the relation between overall closed-loop stability and control gains of this controller is also revealed. Experimental results demonstrate the effectiveness of this current-sensorless controller. In addition, the performance of this current-sensorless controller is compared with that of a full-state feedback controller. Clearly, the proposed current-sensorless controller can achieve zero positioning error within the resolution of an optical encoder. However, the same result is less easy to achieve using a full-state feedback controller due to the noise effect on the current measurements.

Key Words: Permanent Magnet Synchronous Motor, Singular Perturbation, Current Sensorless Control, Two-loop Control, Stability Analysis

1. Introduction

Numerous studies have attempted to simplify the implementation of AC drives. One method reduces the use of measurement sensors, because sensors increase complexity and cost, while reducing the maintainability of a system. Additionally, measurement noises become a problem with an increasing number of sensors. Consequently, reducing the number of sensors in a control system is highly desired. Most sensorless investigations involving permanent magnet synchronous motors (PMSM) have focused on the so-called shaft sensorless control[1]-[8]. Because the shaft-mounted motion sensors are either fragile or bulky, and always expensive, replacing these hardware sensors with software "observers" would be a viable alternative. The shaft-sensorless control methods of PMSMs can be classified into two groups:

1) those based on the back EMF produced in the stator windings;

2) those based on the magnetic saliency of the motor geometry.

Conventional position estimation based on the detection of back EMF is suitable for middle- and high-speed applications. However, at low speed and standstill, the EMF is too small to estimate position accurately[5]. On the other hand, magnetic saliency-based position estimation[6]-[8] can be potentially employed at any speed, including zero speed. However, Mizutani et al.[7] mentioned that the magnetic saliency-based position estimation does not work well in the high-speed range, due to the effect of back EMF.

Unlike shaft-sensorless controls, current-sensorless controls do not have the problem of limited operation speed. Chang and Yeh[9] studied current-sensorless field-oriented control of induction motors, and used a partial state observer to estimate torque current. Matsuo and Lipo[10] proposed a field-oriented control method without current sensors for synchronous reluctance motors. In that study, torque command replaces current variables, then a voltage reference calculator is introduced to generate the required voltage references from the torque command and the

* Received 4th January, 2000

** Department of Mechanical Engineering, National Chiao-Tung University, 1001 Ta-Hsueh Road, Hsin-chu, Taiwan 30010, R.O.C. E-mail: kanping@cc.nctu.edu.tw

motor speed. Chin et al.[11] developed a reduced-order tracking controller, which generates maximum torque in PMSMs. Meanwhile, Chang et al.[12] developed a reduced-order time delay control that is applied to the position control of brushless DC motors. In their works[11],[12], controller designs were based on reduced-order models which are derived from the singular perturbation analysis by exploiting the two-time-scale property of small electrical machines. Controller designs based on these reduced models do not need to measure the current signals for feedback purposes because the model applies a set of second-order nonlinear dynamic equations that contain only mechanical variables. Although the two studies[11],[12] apply singular perturbation analysis[13],[14] to the same mathematical model of PMSM, different reduced-models are derived. This is because different parasitic terms are neglected in their singular perturbation analyses. Computational simplicity is the main feature of the control designs based on reduced-order models; however, the overall closed-loop stabilities with these controllers are hard to be proved. In their works[11],[12], the proofs of the overall closed-loop stability are qualitative only and are based on the assumption that the perturbation scale, ε, which originates in the singular perturbation method, is sufficiently small. The concept of sufficiently small ε is qualitative; therefore, the proofs of stability in their studies[11],[12] are incomplete.

This study first derives a reduced-order model by taking singular perturbation analysis of the mathematical model of a PMSM. A simple and effective position and velocity controller is then developed based on this reduced model. In contrast to a full-state feedback controller, such as the two-loop controller Fig. 1 depicts, this controller does not measure the current signals for feedback purposes. Figures 1

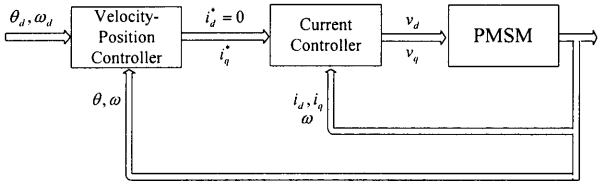

Fig. 1 Block diagram of a two-loop control for the PMSM

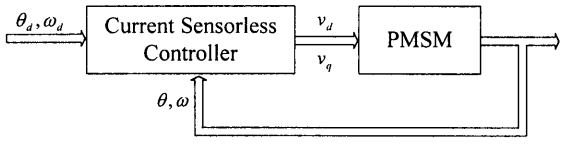

Fig. 2 Block diagram of a current sensorless control for the PMSM

and 2 illustrate the block diagrams of the two-loop controller and the current-sensorless controller respectively. However, this current-sensorless controller can still indirectly control the steady-state d-axis current to zero to minimize power dissipation[15]. Furthermore, to extend the operating speed range when voltage saturation occurs, this controller can generate flux-weakening control with minimum power dissipation automatically[16]. This study investigates the overall closed-loop stability under this controller. The analyses are based on Lyapunov's direct and indirect methods. Experimental results demonstrate the effectiveness of this current-sensorless controller. In addition, the performance of this current-sensorless controller is compared with that of a full-state feedback controller. The proposed current-sensorless controller can clearly achieve zero positioning error within the resolution of an optical encoder. However, the same result is not as easy to achieve with a full-state feedback controller due to noise effect on the current measurements.

The rest of this paper is organized as follows. Section 2 presents the mathematical model of a PMSM. Section 3 derives a reduced model using the singular perturbation method. This section also describes the proposed controller based on this reduced model. The stability analyses are presented in Section 4, while experimental results are presented in Section 5. Conclusions are finally made in Section 6. In the Appendix, a full-state feedback controller based on the feedback linearization method is presented as a comparison to the reduced-order controller developed herein.

2. Mathematical Model of the PMSM

The mathematical model of a smooth air-gap, permanent magnet synchronous motor (SPMSM) in a synchronous frame, or the so-called d-q frame, can be described as follows:

$$\dot{\boldsymbol{x}} = \frac{d}{dt}\begin{Bmatrix}\theta\\ \omega\end{Bmatrix} = \begin{Bmatrix}\omega\\ \left[\frac{3}{2}KNi_q - B\omega - C\,\mathrm{sgn}(\omega)\right]/J\end{Bmatrix} \tag{1}$$

$$\dot{\boldsymbol{i}} = \frac{d}{dt}\begin{Bmatrix}i_d\\ i_q\end{Bmatrix} = \begin{bmatrix}-1/T_e & N\omega\\ -N\omega & -1/T_e\end{bmatrix}\begin{Bmatrix}i_d\\ i_q\end{Bmatrix} + \frac{1}{L}\begin{Bmatrix}v_d\\ v_q - KN\omega\end{Bmatrix} \tag{2}$$

where $\boldsymbol{x} = \{\theta\ \omega\}^T$ represents the mechanical state vector whose components are the rotor position and rotor velocity, respectively; $\boldsymbol{i} = \{i_d\ i_q\}^T$ denotes the electrical state vector in the d-q frame, and the components of $\boldsymbol{i}$ are the direct-axis and the quadrature-axis stator currents respectively; $\boldsymbol{v} = \{v_d\ v_q\}^T$ represents the input vector whose components

are input voltages in the d-q frame; L is the phase inductance; R denotes the phase resistance; $T_e = L/R$ denotes the electrical time constant; N denotes the number of pole pairs; K represents the torque (permanent magnet) constant; J is the rotor inertia; B denotes the viscous damping coefficient; and C represents the Coulomb friction coefficient. With a full-state feedback controller, the input vector is a function of time, electrical states, and mechanical states, i.e., $\boldsymbol{v}=\boldsymbol{v}(t, \boldsymbol{i}, \boldsymbol{x})$. Since this study aims to achieve position or velocity controls without using the current information, the input vector is constrained to a function of time and the mechanical states, i.e., $\boldsymbol{v}=\boldsymbol{v}(t, \boldsymbol{x})$. Moreover, because the term C sign(ω) in Eq. (1) is discontinuous at $\omega=0$, the following discussions will ignore the operation region, $\omega=0$, to simplify the analysis.

3. Control Strategies

3.1 Reduced order modeling

The two-time-scale phenomenon of small electrical machines is manifested by the fact that the time constant of the electrical subsystem, T_e, is significantly smaller than that of the mechanical subsystem, J/B. Hence, by assigning a small positive constant $\varepsilon = T_e$ and assuming $\omega \neq 0$, the motor model (1), (2) can be re-expressed as a standard singular perturbation form[13),14)] by multiplying ε to both sides of the electrical subsystem (2):

$$\begin{Bmatrix} \dot{\theta} \\ \dot{\omega} \end{Bmatrix} = \begin{Bmatrix} \omega \\ \dfrac{3KN}{2J} i_q - \dfrac{B}{J}\omega - \dfrac{C}{J}\operatorname{sgn}(\omega) \end{Bmatrix} \tag{3}$$

$$\varepsilon \begin{Bmatrix} \dot{i}_d \\ \dot{i}_q \end{Bmatrix} = \begin{bmatrix} -1 & T_e N\omega \\ -T_e N\omega & -1 \end{bmatrix} \begin{Bmatrix} i_d \\ i_q \end{Bmatrix} + \frac{1}{R} \begin{Bmatrix} v_d \\ v_q - KN\omega \end{Bmatrix} \tag{4}$$

Notably, in Eq. (4), although T_e is a small number, the term $T_e N\omega$ may not be a small number when $N\omega$ is large. Therefore, $T_e N\omega$ cannot be considered a negligible parasitic term.

The singular perturbation analysis of system (3), (4) was studied by Chen and Chin[15]. Suppose electrical subsystem (4) reaches its quasi-steady-state instantaneously. The quasi-steady-state of the electrical variables can be determined by substituting $\varepsilon = 0$ in Eq. (4):

$$\begin{Bmatrix} \bar{i}_d \\ \bar{i}_q \end{Bmatrix} = \frac{1}{DL} \begin{Bmatrix} (v_q - KN\omega)N\omega + v_d/T_e \\ -(v_d + K/T_e)N\omega + v_q/T_e \end{Bmatrix} \tag{5}$$

where, $D = N^2\omega^2 + 1/T_e^2$, and $\bar{i}_d$ and $\bar{i}_q$ are the quasi-steady-state values of i_d and i_q, respectively. Replacing i_q in Eq. (3) with its quasi-steady-state $\bar{i}_q$ allows us to obtain a reduced model of the full system (3), (4):

$$\begin{Bmatrix} \dot{\theta} \\ \dot{\omega} \end{Bmatrix} = \begin{Bmatrix} \omega \\ \dfrac{3KN}{2J} \bar{i}_q - \dfrac{B}{J}\omega - \dfrac{C}{J}\operatorname{sgn}(\omega) \end{Bmatrix} \tag{6}$$

The reduced model (6) is described by a set of nonlinear second-order differential equations in which the states are the same as the states of the mechanical subsystem in the full model (3), (4).

3.2 Control law design

Because the d-axis current, i_d, does not generate torque in a SPMSM system, it is commanded to become zero under normal operating conditions to reduce the power dissipation from the winding resistance. However, because i_d is not a state in the reduced model, to achieve near minimum power dissipation, we will command $\bar{i}_d$ to zero instead. By substituting $\bar{i}_d = 0$ into Eq. (5), the relationship between v_d and v_q that produces this steady-state d-axis current can be solved as

$$v_d = T_e N\omega(KN\omega - v_q) \tag{7}$$

Furthermore, by substituting Eq. (7) into (5), $\bar{i}_q$, which produces the desired steady-state q-axis current, can also be computed. Consequently, the reduced model (6) can be rewritten as the following form by substituting $\bar{i}_q$ into Eq. (6):

$$v_q = \frac{2JR}{3KN}\dot{\omega} + \left(\frac{2BR}{3KN} + KN\right)\omega + \frac{2CR}{3KN}\operatorname{sgn}(\omega) \tag{8}$$

Based on Eq. (8), a feedback linearization control law can be chosen as follows:

$$v_q = \frac{2JR}{3KN}(\dot{\omega}_d - \lambda_\omega e_\omega - \lambda_\theta e_\theta - \lambda_\varphi e_\varphi) + \left(\frac{2BR}{3KN} + KN\right)\omega + \frac{2CR}{3KN}\operatorname{sgn}(\omega) \tag{9}$$

where, $e_\omega = \omega - \omega_d$, $e_\theta = \theta - \theta_d$, $e_\varphi = \int e_\theta dt$, θ_d and ω_d are the desired position and desired velocity respectively, and, λ_ω, λ_θ and λ_φ are constant control gains. By substituting the control law (9) into the reduced model (8), the closed-loop error dynamics of the reduced-order system becomes

$$\begin{cases} \dot{e}_\varphi = e_\theta \\ \dot{e}_\theta = e_\omega \\ \dot{e}_\omega = -\lambda_\omega e_\omega - \lambda_\theta e_\theta - \lambda_\varphi e_\varphi \end{cases} \tag{10}$$

The eigenvalues of Eq. (10), $-\sigma_a$, $-\sigma_b$ and $-\sigma_c$, can be designated by selecting the control gains as follows:

$$\begin{cases} \lambda_\omega = \sigma_a + \sigma_b + \sigma_c, \\ \lambda_\theta = \sigma_a\sigma_b + \sigma_b\sigma_c + \sigma_a\sigma_c, \\ \lambda_\varphi = \sigma_a\sigma_b\sigma_c. \end{cases} \tag{11}$$

The eigenvalues can be either all real numbers, or one real number plus a pair of complex conjugate numbers. Consequently, the equilibrium point of the reduced model (6) is globally exponentially stable under the control law (7) and (9), as long as the real parts of, σ_a, σ_b and σ_c are all positive; or equivalently, the control gains, λ_φ, λ_θ and λ_ω, are all positive.

4. Stability Analyses

Although the above-mentioned controller is designed to stabilize the reduced model, it remains uncertain whether or not the controller will be able to stabilize the original full model in the presence of the fast (electrical) dynamics, which have been assumed to be instantaneous. Numerous investigations have addressed the stability problem of singularly perturbed systems [13),(14),(17)-(21)]. Ioannou and Kokotovic[17], and Taylor et al.[18] studied qualitative analyses of the robustness with respect to singularly perturbed systems. Corless and Glielmo [19], and theorem 9.3[14] both established robustness of systems that contain exponentially stable unmodeled fast dynamics. Meanwhile, Saberi and Khalil[20] developed scalar quadratic-type Lyapunov functions to perform the stability analysis of nonlinear singularly perturbed systems. Using this method, a stable operation region is defined and the upper bound of sufficiently small ε is found. However, the stable operation region developed therein is local and dependent on the choice of the Lyapunov function, which cannot be found systematically. Retchkiman and Silva[21] proposed a method that used vector Lyapunov functions and comparison principles for stability analysis of nonlinear singularly perturbed systems. However, with this method, finding suitable Lyapunov functions remains a major obstacle.

This section first presents a Lyapunov function that can prove the global asymptotic stability of the proposed control method when the control gains are limited to a given range. Moreover, supplemented with Lyapunov's linearization analysis, we can show that the proposed control possesses high-gain instability. Accordingly, the set of control gains, $(\lambda_\varphi, \lambda_\theta, \lambda_\omega)$, must be carefully chosen to avoid instability.

4.1 Lyapunov's direct method

This subsection employs Lyapunov's direct method to prove the stability of the overall system. By substituting Eqs.(7) and (9) into the original model (1) and (2) while assuming ω_d be a constant, the closed-loop error dynamics of the full system becomes

$$\begin{cases} \dot{e}_\varphi = e_\theta \\ \dot{e}_\theta = e_\omega \\ \dot{e}_\omega = \dfrac{3KN}{2J}\tilde{i}_q - \lambda_\omega e_\omega - \lambda_\theta e_\theta - \lambda_\varphi e_\varphi \end{cases} \tag{12}$$

$$\begin{cases} \dot{\tilde{i}}_d = -\dfrac{1}{T_e}\tilde{i}_d + N(e_\omega + \omega_d)\tilde{i}_q \\ \dot{\tilde{i}}_q = -N(e_\omega + \omega_d)\tilde{i}_d - \dfrac{1}{T_e}\tilde{i}_q \\ \quad -\left(\dfrac{2B}{3KN} - \dfrac{2J}{3KN}\lambda_\omega\right)\dot{e}_\omega + \dfrac{2J}{3KN}(\lambda_\theta e_\omega + \lambda_\varphi e_\theta) \end{cases} \tag{13}$$

where $\tilde{i}_d = i_d - \bar{i}_d$ and $\tilde{i}_q = i_q - \bar{i}_q$. The system described by Eqs.(12) and (13) is an autonomous nonlinear system, and its origin is a unique equilibrium point. To prove the stability, a quadratic-type Lyapunov function candidate is chosen as the following:

$$V = \frac{1}{2}\{e_\varphi \quad e_\theta \quad e_\omega\}\boldsymbol{P}\begin{Bmatrix} e_\varphi \\ e_\theta \\ e_\omega \end{Bmatrix} + \frac{1}{2}\tilde{i}_d^2 + \frac{1}{2}\tilde{i}_q^2 \tag{14}$$

where

$$\boldsymbol{P} = \begin{bmatrix} P_{11} & P_{12} & P_{13} \\ P_{12} & P_{22} & P_{23} \\ P_{13} & P_{23} & P_{33} \end{bmatrix}$$

is a constant symmetric matrix. The necessary and sufficient conditions that make the Lyapunov function candidate (14) positive definite are

$$P_{11} > 0, \tag{15}$$

$$\det\begin{bmatrix} P_{11} & P_{12} \\ P_{12} & P_{22} \end{bmatrix} > 0, \tag{16}$$

$$\det\begin{bmatrix} P_{11} & P_{12} & P_{13} \\ P_{12} & P_{22} & P_{23} \\ P_{13} & P_{23} & P_{33} \end{bmatrix} > 0 \tag{17}$$

Obviously, this Lyapunov function candidate is radically unbounded. Taking the time derivative of the Lyapunov function candidate (14) along the dynamics (12), (13) produces

$$\begin{aligned} \dot{V} &= (-P_{13}\lambda_\varphi)e_\varphi^2 + (P_{12} - P_{23}\lambda_\theta)e_\theta^2 + (P_{23} - P_{33}\lambda_\omega)e_\omega^2 \\ &\quad + \left(-\frac{1}{T_e}\right)\tilde{i}_d^2 + \left(-\frac{1}{T_e} - \frac{3KN}{2J}A\right)\tilde{i}_q^2 \\ &\quad + (P_{11} - P_{13}\lambda_\theta - P_{23}\lambda_\varphi)e_\varphi e_\theta \\ &\quad + (P_{12} - P_{13}\lambda_\omega - P_{33}\lambda_\varphi)e_\varphi e_\omega \\ &\quad + (P_{22} + P_{13} - P_{33}\lambda_\theta - P_{23}\lambda_\omega)e_\theta e_\omega \\ &\quad + \left(\frac{3KN}{2J}P_{13} + A\lambda_\varphi\right)e_\varphi \tilde{i}_q \\ &\quad + \left(\frac{3KN}{2J}P_{23} + A\lambda_\theta + \frac{2J}{3KN}\lambda_\varphi\right)e_\theta \tilde{i}_q \\ &\quad + \left(\frac{3KN}{2J}P_{23} + A\lambda_\omega + \frac{2J}{3KN}\lambda_\theta\right)e_\omega \tilde{i}_q \\ &= c_1 e_\varphi^2 + c_2 e_\theta^2 + c_3 e_\omega^2 + \left(-\frac{1}{T_e}\right)\tilde{i}_d^2 + c_4 \tilde{i}_q^2 \\ &\quad + c_5 e_\varphi e_\theta + c_6 e_\varphi e_\omega + c_7 e_\theta e_\omega + c_8 e_\varphi \tilde{i}_q \\ &\quad + c_9 e_\theta \tilde{i}_q + c_{10} e_\omega \tilde{i}_q \end{aligned} \tag{18}$$

where $A = \left(\dfrac{2B}{3KN} - \dfrac{2J}{3KN}\lambda_\omega\right)$. If $\dot{V}$ is negative definite, then the equilibrium point of (12), (13) is globally asymptotically stable. To make $\dot{V}$ negative definite, the coefficients, $c_1, \cdots, c_4$ are chosen to be negative, and the coefficients, $c_5, \cdots, c_{10}$, are chosen to be equal to zero. By setting the coefficients, $c_5, \cdots, c_{10}$, to zero, the elements of the matrix $\boldsymbol{P}$ can be obtained as follows:

$$P_{13} = -\frac{2J}{3KN}A\lambda_\varphi,$$

$$P_{23}=-\frac{2J}{3KN}\left(A\lambda_\theta+\frac{2J}{3KN}\lambda_\varphi\right),$$
$$P_{33}=-\frac{2J}{3KN}\left(A\lambda_\omega+\frac{2J}{3KN}\lambda_\theta\right), \quad (19)$$
$$P_{11}=P_{13}\lambda_\theta+P_{23}\lambda_\varphi,$$
$$P_{12}=P_{13}\lambda_\omega+P_{33}\lambda_\varphi,$$
$$P_{22}=-P_{13}+P_{33}\lambda_\theta+P_{23}\lambda_\omega.$$

Additionally, letting the coefficients, $c_1, \cdots, c_4$, be negative numbers produces the following constraints:

$$c_1<0 \Rightarrow -P_{13}\lambda_\varphi<0 \quad (20)$$
$$c_2<0 \Rightarrow P_{12}-P_{23}\lambda_\theta<0 \quad (21)$$
$$c_3<0 \Rightarrow P_{23}-P_{33}\lambda_\omega<0 \quad (22)$$
$$c_4<0 \Rightarrow -\frac{1}{T_e}-\frac{3KN}{2J}A<0 \quad (23)$$

The range of control gains, λ_ω, λ_θ and λ_φ, that globally stabilize (12), (13) can be computed from the constraint equations (15)-(17) and (20)-(23). Because the set of eigenvalues, $(\sigma_a, \sigma_b, \sigma_c)$, represents the bandwidth of error convergence of the reduced closed-loop system (10), it seems more helpful to understand the stability property of the suggested control by replacing the set of control gains $(\lambda_\varphi, \lambda_\theta, \lambda_\omega)$ in the above conditions with $(\sigma_a, \sigma_b, \sigma_c)$ according to Eq.(11). Furthermore, by letting $\sigma_a=\sigma_b=\sigma_c=\sigma$, the analysis can be simplified and a range of σ that satisfies each condition can be derived. Finally, a range of σ that can globally stabilize the error dynamics of the full-order system (12), (13) can be obtained by intersecting the ranges of σ derived individually from conditions(15)-(17) and (20)-(23). By substituting the identified motor parameters, listed in Table 1, into the constraint equations, the stable range of σ is derived as

$$0.7442<\sigma<200.301 \quad (24)$$

Notably, the stable range of σ is derived using Lyapunov's direct method; as a result, it is only a sufficient condition to guarantee the globally asymptotic stability of the unique equilibrium point at the origin of the system described by Eqs.(12) and (13). The global asymptotic stability of the origin also indicates that the control goals, $e_\theta=0$, $e_\omega=0$, and $\tilde{i}_d=i_d-\bar{i}_d=0$, are attainable.

Besides its globally asymptotic stability, the proposed controller is also robust. The robustness comes from using the integration of position error, e_φ, in the control law. Therefore, small parameter uncertainties will not affect the achievement of the control goals of $e_\theta=0$ and $e_\omega=0$.

4.2 Lyapunov's linearization method

The local stability of system (12) and (13) can be further analyzed by linearizing (12) and (13) around its equilibrium point. Figures 3(a), (b), (c) illustrate the loci of eigenvalues of (12) and (13) by varying ω_d from 10 rpm to 3 000 rpm. As in the above stability analysis, σ_a, σ_b and σ_c are given equal values, σ, at 5 Hz, 30 Hz, and 60 Hz for Figs. 3(a), 3(b) and 3(c) respectively. One set of two loci on the left-hand side of Fig. 3(a) are eigenvalues of the linearized electrical subsystem, while the other set of three loci on the right-hand side of Fig. 3(a) are

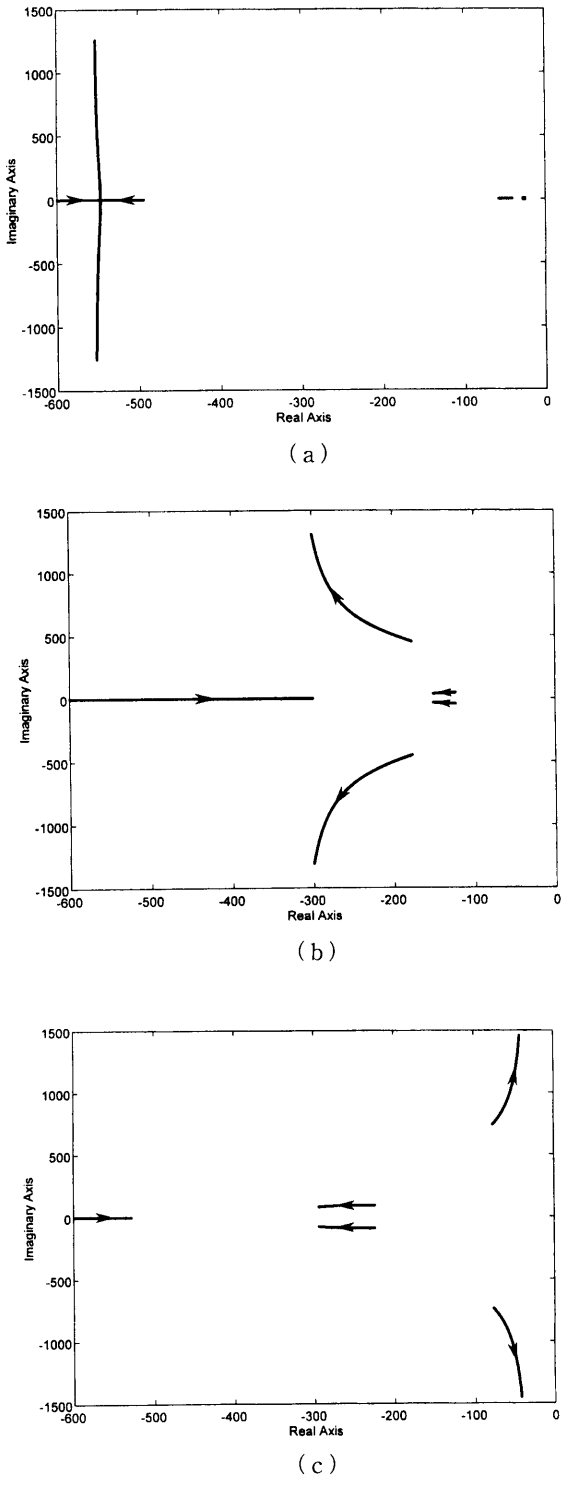

Fig. 3 Loci of eigenvalues when $\omega_d=10\sim3\,000$ rpm and (a) $\sigma=5$ Hz; (b) $\sigma=30$ Hz; (c) $\sigma=60$ Hz

eigenvalues of the linearized mechanical subsystem. In Figs. 3(b) and 3(c), where σ is increased to 30 Hz and 60 Hz, respectively, the set of loci representing eigenvalues of the linearized electrical subsystem move toward the imaginary axis and to the right of the set of loci representing eigenvalues of the linearized mechanical subsystem. Furthermore, when σ increases beyond a certain value, the set of loci representing eigenvalues of the linearized electrical subsystem will move into the right half-plane and the linearized system will become unstable. According to Lyapunov's linearization method, if the linearized system is unstable, then the equilibrium point of the original nonlinear system will be unstable. Therefore, combining the results of Lyapunov's linearization analysis with the results of Lyapunov's direct analysis, it can be concluded that the value of stabilizing σ evidently has an upper bound. Restated, the proposed current sensorless control possesses high-gain instability and the control gains must be both lower- and upper-bounded. Consequently, the set of control gains, $(\lambda_\varphi, \lambda_\theta, \lambda_\omega)$, must be carefully and conservatively chosen to comply with the bounds on the eigenvalues.

5. Experimental Results

The experimental setup includes a Sinano #7CB30-2SE6F permanent magnet synchronous motor, the power stage of a Micro Trend UT90 driver, a proprietary control card made in-house, and a PC. The control card converts the analog phase current measurements into digital signals, decodes the encoder signals and the Hall effect sensor signals, and generates space vector pulse width modulation (SVPWM) switching signals to control the power stage. The PC is used to compute the control algorithms and the coordinate transformations among the vector space, stator reference frame, and rotor reference frame. The experiments compare the control performances of the proposed current-sensorless controller with those of a full-state feedback controller. The design and stability analysis of this full-state feedback controller are presented in the Appendix for comparison. Similar to the current-sensorless controller, the d-axis current command in the full-state feedback controller is also set to zero. The control gains corresponding to the eigenvalues of the mechanical subsystem at $\sigma_a=\sigma_b=\sigma_c=30$ Hz, which are in the stable range of Eq.(24), are selected for both controllers. Additionally, the full-state feedback controller is implemented in a two-loop control structure, as Fig. 1 illustrates, in which the bandwidth of the current controller is ten times that of the velocity-position controller. Besides, multi-sampling rates of 1 kHz and 10 kHz are employed in the full-state feedback controller, in contrast to the unitary sampling rate of 5 kHz used in the current-sensorless controller. Furthermore, the identified motor parameters, as shown in Table 1, are used in the two controllers in the experiments. To show the positioning capability of the current-sensorless controller, a velocity trajectory command that contains a zero-speed region is implemented, as Fig. 4 illustrates. The position command is the integration of this velocity command. Nevertheless, the position command must be quantized according to the resolution of the optical encoder to avoid the meaningless integration of position error in the zero-speed command region. The resolution of the optical encoder mounted on the applied motor is 8 000 counts per revolution. In addition, because the Coulomb friction term, $C\,\mathrm{sgn}(\omega)$, in the feedback linearization control laws will induce output oscillation when the velocity fluctuates around zero, it is removed from the control laws when the velocity command is zero.

Figures 5 and 6 present the experimental results of the current-sensorless control and the full-state feedback control, respectively. The current-sensorless control has greater control errors, e_θ, e_ω and i_d, than the full-state feedback control in the acceleration and the deceleration regions, as revealed by comparing Figs. 5(a), (b), (c) with Figs. 6(a), (b), (c). However, as observed in Fig. 5(a), the position error converges to zero in the zero-speed region when the current-sensorless controller is implemented. This phenomenon implies that the current-sensorless controller can achieve positioning precision to the

Table 1 Identified parameters of the Sinano #7CB30-2SE6F motor

Pole pair	$N = 4$
Resistance	$R = 3.55\,(\Omega)$
Inductance	$L = 5.92\times10^{-3}$ (H)
Magnet constant	$K = 5.795\times10^{-2}$ (V · sec/rad)
Rotor inertia	$J = 6.45\times10^{-5}$ (kg · m^2)
Viscous damping coefficient	$B = 8\times10^{-5}$ (N · m · sec/rad)
Column friction coefficient	$C = 1.738\times10^{-2}$ (N · m)

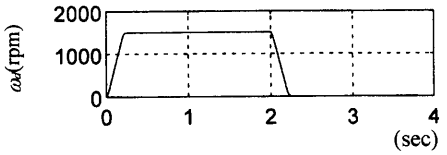

Fig. 4 Trajectory of the velocity command in experimentation

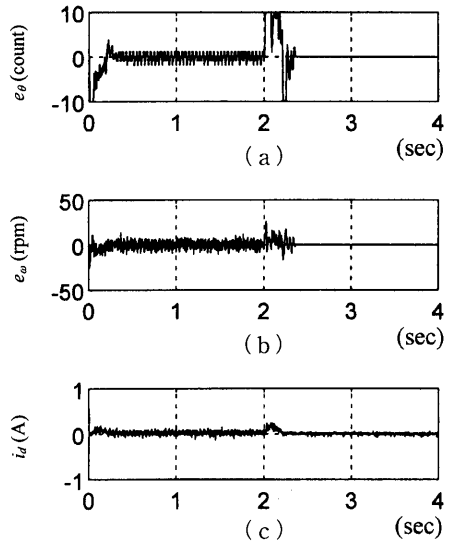

Fig. 5 Results of the tracking experiment with the current sensorless controller. (a) position error, (b) velocity error, (c) d-axis current

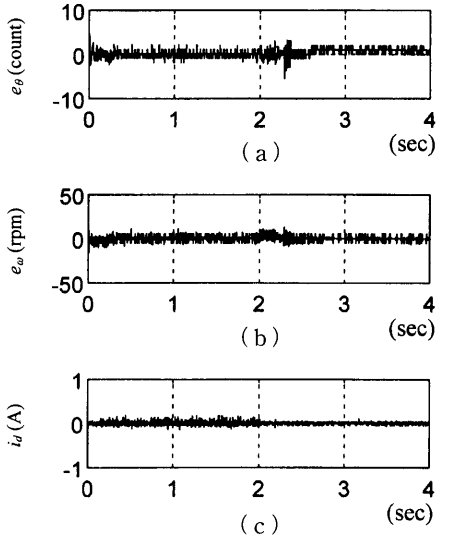

Fig. 6 Results of the tracking experiment with the full-state feedback controller. (a) position error, (b) velocity error, (c) d-axis current

minimum measuring unit of a position measurement device, such as an optical encoder. In contrast, the position error of the full-state feedback controller in the zero-speed region, as shown in Fig. 6(a), is oscillating within a small range. The oscillation is largely attributed to the effect of noises that enter the current controller via current measurement feedback. Because phase currents should be small when the motor is running at low speed and not under load, the noises will dominate the measured current in the near-zero-speed regions. Consequently, at low speed the current controller will track the noises and simultaneously generate small velocity oscillation. However, the problem of noise corruption in the current measurements can be avoided entirely by using a current-sensorless controller because the current signals are unnecessary for feedback purposes.

6. Conclusions

This study analyzes the stability of a simple and effective current-sensorless controller for a PMSM control system. By using Lyapunov's direct method, it shows that this controller is globally asymptotically stable when the control gains are limited to a certain range. By combining this result with the result from Lyapunov's linearization analysis, we conclude that this controller possesses high-gain instability and the control gains must be both upper- and lower bounded. Although this controller does not need the current information of the motor for feedback, the steady-state d-axis current can still be controlled to zero to minimize power dissipation. Experimental results confirm that the proposed current-sensorless controller can indeed achieve position and velocity control with zero steady-state d-axis current. Moreover, experimental results also indicate that the current-sensorless controller can achieve zero positioning error within the resolution of an optical encoder. However, the same result is harder to achieve by using a full-state feedback controller due to noise effect on the current measurements.

Appendix: Full-State Feedback Control Design

A. Control Law Design

Consider the mechanical subsystem (1) of the motor model. If Eq.(1) is treated as an independent system, the q-axis current i_q in Eq.(1) can be considered as a virtual control. A feedback linearization control law for Eq.(1) can be chosen as follows:

$$i_q=\frac{2J}{3KN}\left[\frac{B}{J}\omega+\frac{C}{J}\operatorname{sgn}(\omega)+\dot{\omega}_d-\lambda_\omega e_\omega -\lambda_\theta e_\theta-\lambda_\varphi e_\varphi\right] \tag{25}$$

Consequently, the responses e_ω, e_θ and e_φ can be adjusted by tuning the control gains, λ_ω, λ_θ, and λ_φ according to the relations of the closed-loop eigenvalues and the control gains in Eq.(11). However, because i_q is just a state variable of the full model (1), (2) and not the control input, i_q can be replaced with its desired value i_q^* in Eq.(25). Taking i_q^* as a command input for the electrical subsystem (2), feedback linearization current control laws for Eq.(2) can be chosen as

$$v_d=L\left(\frac{1}{T_e}i_d-N\omega i_q+\dot{i}_d^*-\lambda_{dp}e_d-\lambda_{di}e_{d\text{-}i}\right) \tag{26}$$

$$v_q=L\left(N\omega i_d+\frac{1}{T_e}i_q+\dot{i}_q^*-\lambda_{qp}e_q-\lambda_{qi}e_{q\text{-}i}\right)+KN\omega \tag{27}$$

where i_d^* denotes the d-axis current command; $e_d=i_d-i_d^*$ and $e_q=i_q-i_q^*$ are d- and q-axis current errors, respectively; $e_{d\text{-}i}=\int e_d dt$ and $e_{q\text{-}i}=\int e_q dt$; and λ_{dp}, λ_{di}, λ_{qp}, and λ_{qi} are control gains. Because control laws (26) and (27) decouple the dynamics of the d-axis and the q-axis, i_d and i_q can have independent error dynamics. These two error dynamics can be designated by tuning the control gains as follows:

$$\begin{cases}\lambda_{dp}=\sigma_{da}+\sigma_{db}\\ \lambda_{di}=\sigma_{da}\sigma_{db}\end{cases} \tag{28}$$

$$\begin{cases}\lambda_{qp}=\sigma_{qa}+\sigma_{qb}\\ \lambda_{qi}=\sigma_{qa}\sigma_{qb}\end{cases} \tag{29}$$

where $-\sigma_{da}$ and $-\sigma_{db}$ are the designated eigenvalues of the closed-loop d-axis current error dynamics, and $-\sigma_{qa}$ and $-\sigma_{qb}$ are the designated eigenvalues of the closed-loop q-axis current error dynamics. Generally, σ_{da} and σ_{db} are chosen to equal σ_{qa} and σ_{qb}, respectively, during implementation, such that i_d and i_q will have the same closed loop error dynamics.

B. Overall Stability Analysis

By substituting control laws (26) and (27) into system (1), (2), the overall closed-loop error dynamics becomes a linear system:

$$\frac{d}{dt}\begin{Bmatrix}e_\varphi\\ e_\theta\\ e_\omega\\ e_{d\text{-}i}\\ e_d\\ e_{q\text{-}i}\\ e_q\end{Bmatrix}=\begin{bmatrix}0&1&0&0&0&0&0\\ 0&0&1&0&0&0&0\\ -\lambda_\varphi&-\lambda_\theta&-\lambda_\omega&0&0&0&\frac{3KN}{2J}\\ 0&0&0&0&1&0&0\\ 0&0&0&-\lambda_{di}&-\lambda_{dp}&0&0\\ 0&0&0&0&0&0&1\\ 0&0&0&0&0&-\lambda_{qi}&-\lambda_{qp}\end{bmatrix}\begin{Bmatrix}e_\varphi\\ e_\theta\\ e_\omega\\ e_{d\text{-}i}\\ e_d\\ e_{q\text{-}i}\\ e_q\end{Bmatrix} \tag{30}$$

The eigenvalues of Eq.(30) are, $-\sigma_a$, $-\sigma_b$, $-\sigma_c$, $-\sigma_{da}$, $-\sigma_{db}$, $-\sigma_{qa}$, and $-\sigma_{qb}$. Provided the eigenvalues of Eq.(30) are all placed on the left half-plane of the complex space, or equivalently, the control gains in Eq.(30) are all positive numbers, the origin of Eq.(30) is globally exponentially stable. Additionally, if the real part of the eigenvalues of the electrical subsystem, $-\sigma_{qa}$, and $-\sigma_{qb}$, are much smaller than the real part of the eigenvalues of the mechanical subsystem, $-\sigma_a$, $-\sigma_b$, and $-\sigma_c$, then the electrical state i_q will rapidly converge to its desired value i_q^*, and the responses, e_ω, e_θ and e_φ can be completely described by the eigenvalues $-\sigma_a$, $-\sigma_b$, and $-\sigma_c$.

The full-state feedback controller developed above is very similar to the conventional two-loop controller[22]. Nevertheless, these two controllers are subtly different. Both controllers contain the terms $N\omega i_q$ and $N\omega i_d$ in the current control laws to decouple the electrical dynamics of the d-axis and the q-axis. However, the conventional two-loop controller does not contain the derivative of the current commands, i_d^* and i_q^*, as in Eqs.(26) and (27). Without these two terms, the zero steady-state error is only guaranteed for constant current commands. Moreover, from the viewpoint of two-time-scale systems, if the convergence rate of the current loop is sufficiently faster than that of the mechanical loop, the overall stability of the conventional two-loop design can be proven via the singular perturbation method. Consequently, a conventional two-loop controller is stable only when both loops are stable and the inner (current) loop is much faster than the outer (mechanical) loop.

References

(1) Jones, L.A. and Lang, J.H., A State Observer for the Permanent-Magnet Synchronous Motor, IEEE Trans. on Ind. Electr., Vol. 36, No. 3 (1989), pp. 374-382.

(2) Sepe, R.B. and Lang, J.H., Real-Time Observer-Based (Adaptive) Control of A Permanent-Magnet Synchronous Motor without Mechanical Sensors, IEEE Trans. on Ind. Appl., Vol. 28, No. 6 (1992), pp. 1345-1352.

(3) Solsona, J., Valla, M.I. and Muravchik, C., Nonlinear Reduced Order Observer for Permanent Magnet Synchronous Motors, Proc. of the IEEE 20th. Int. Conf. on Industrial Electronics Control and Instrumentation, (IECON '94), pp. 38-43.

(4) Hofmann, H. and Sanders, S.R., Speed-Sensorless Vector Torque Control of Induction Machines Using a Two-Time-Scale Approach, IEEE Trans. on Ind. Appl., Vol. 34, No. 1 (1998), pp. 169-177.

(5) Shouse, K.R. and Taylor, D.G., Sensorless Velocity Control of Permanent-Magnet Synchronous Motor, IEEE Trans. on Control Systems Technology, Vol. 6, No. 3 (1998), pp. 313-324.

(6) Corley, M.J. and Lorenz, R.D., Rotor Position and Velocity Estimation for a Salient-Pole Permanent Magnet Synchronous Machine at Standstill and High Speeds, IEEE Trans. on Ind. Appl., Vol. 34, No. 4 (1998), pp. 784-789.

(7) Mizutani, R., Takeshita, T. and Matsui, N., Current Model-Based Sensorless Drives of Salient-

Pole PMSM at Low Speed and Standstill, IEEE Trans. on Ind. Appl., Vol. 34, No. 4 (1998), pp. 841-846.
(8) Ogasawara, S. and Akagi, H., An Approach to Real-Time Position Estimation at Zero and Low Speed for a PM Motor Based on Saliency, IEEE Trans. on Ind. Appl., Vol. 34, No. 1 (1998), pp. 163-168.
(9) Chang, S.-C. and Yeh, S.-N., Current Sensorless Field-Oriented Control of Induction Motors, IEE Proc. Electr. Power Appl., Vol. 143, No. 6 (1996), pp. 492-500.
(10) Matsuo, T. and Lipo, T.A., Current Sensorless Field Oriented Control of Synchronous Reluctance Motor, IEEE Ind. Appl. Conf. 28th IAS Annual Meeting, Vol. 1 (1993), pp. 672-678.
(11) Chin, K.-P., Huang, S.-J., Ilic, M. and Zobian, A., Nonlinear Tracking Control of Small Electrical Machines, Proc. 33th IEEE CDC., Vol. 1 (1994), pp. 211-212.
(12) Chang, P.H., Lee, J.H. and Park, S.H., A Reduced Order Time-Delay Control for Highly Simplified Brushless DC Motor, Proc. of the American Control Conference, Vol. 6 (1998), pp. 3791-3795.
(13) Kokotovic, P.V., Khalil, H.K. and O'Reilly, J., Singular Perturbation Methods in Control: Analysis and Design, (1986), Chap. 1, Academic Press, London.
(14) Khalil, H.K., Nonlinear Systems, 2nd ed., (1996), Chap. 9, Prentice-Hall, New Jersey.
(15) Chen, J.-J. and Chin, K.-P., Reduced-Order Control of Permanent Magnet Synchronous Motors, IECON, Vol. 3 (1999), pp. 1361-1366.
(16) Chen, J.-J. and Chin, K.-P., Automatic Flux-Weakening Control of Permanent Magnet Synchronous Motors Using a Reduced-Order Controller, IEEE Trans. on Power Electronics, Vol. 15, No. 5 (2000), pp. 881-890..
(17) Ioannou, P.A. and Kokotovic, P.V., Robust Redesign of Adaptive Control, IEEE Trans. Aut. Contr., Vol. AC-29 (1984), pp. 202-211.
(18) Taylor, D.G., Kokotovic, P.V., Marino, R. and Kanellakopoulos, I., Adaptive Regulation of Nonlinear Systems with Unmodeled Dynamics, IEEE Trans. Aut. Contr., Vol. AC-34 (1989), pp. 405-412.
(19) Corless, M. and Glielmo, L., Robustness of Output Feedback for a Class of Singularly Perturbed Nonlinear Systems, Proc. 30th IEEE CDC., Vol. 2 (1991), pp. 1066-1071.
(20) Saberi, A. and Khalil, H.K., Quadratic-Type Lyaupnov Functions for Singularly Perturbed Systems, IEEE Trans. Aut. Control, Vol. AC-29 (1984), pp. 542-550.
(21) Retchkiman, Z. and Silva, G., Stability Analysis of Singularly Perturbed Systems via Vector Lyapunov Methods, Proc. 35th IEEE CDC., Vol. 1 (1996), pp. 580-585.
(22) Sepe, R.B. and Lang, J.H., Real-Time Adaptive Control of the Permanent-Magnet Synchronous Motor, IEEE Trans. on Ind. Appl., Vol. 27, No. 4 (1991), pp. 706-714.